Graphical Abstract

Fabrication of Nd- and Ce-doped uranium dioxide microspheres via internal gelation

Christian Schreinemachers, Gregory Leinders, Giuseppe Modolo, Marc Verwerft, Koen Binnemans, Thomas Cardinaels

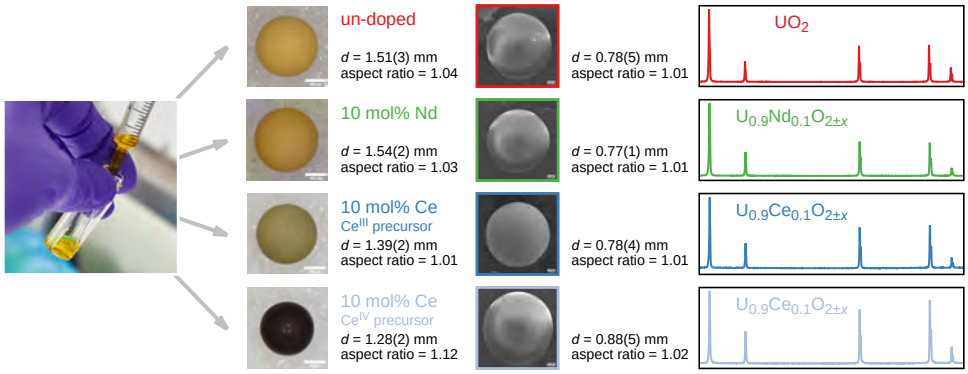

Fabrication of Nd- and Ce-doped uranium dioxide microspheres via internal gelation
C. Schreinemachers, G. Leinders, G. Modolo, M. Verwerft, K. Binnemans, T. Cardinaels
Journal of Nuclear Materials 535 (2020) 152128
DOI: 10.1016/j.jnucmat.2020.152128

Highlights

Fabrication of Nd- and Ce-doped uranium dioxide microspheres via internal gelation

Christian Schreinemachers, Gregory Leinders, Giuseppe Modolo, Marc Verwerft, Koen Binnemans, Thomas Cardinaels

- Nd- and Ce-doped gels with *Ln* contents up to 30 mol% and good sphericity synthesised
- successful implementation of the dopant into $3UO_3{\cdot}2NH_3{\cdot}4H_2O$ matrix of the gel
- Ce^{III} more suitable than Ce^{IV} for the fabrication of doped UO_2 by internal gelation
- single phases for $U_{0.95}Ln_{0.05}O_{2\pm x}$ to $U_{0.7}Nd_{0.3}O_{2\pm x}$ and $U_{0.8}Ce_{0.2}O_{2\pm x}$ obtained
- fabrication process for transmutation fuel or targets materials via IG improved

Fabrication of Nd- and Ce-doped uranium dioxide microspheres via internal gelation

Christian Schreinemachers[a,b,*], Gregory Leinders[a], Giuseppe Modolo[c], Marc Verwerft[a], Koen Binnemans[b], Thomas Cardinaels[a,b]

[a] *Belgian Nuclear Research Centre (SCK CEN), Institute for Nuclear Materials Science, Boeretang 200, B-2400 Mol, Belgium*
[b] *KU Leuven, Department of Chemistry, Celestijnenlaan 200F, P.O. Box 2404, B-3001 Heverlee, Belgium*
[c] *Forschungszentrum Jülich GmbH, Institute of Energy and Climate Research, IEK-6: Nuclear Waste Management and Reactor Safety, 52425 Jülich, Germany*

Abstract

The sol-gel route via internal gelation was applied for the production of Nd- and Ce-doped uranium dioxide microspheres. Trivalent and tetravalent Ce precursors were used and the influence of the precursors' oxidation state on the fabrication process and the final product was studied. The successful introduction of the dopant into the $3UO_3{\cdot}2NH_3{\cdot}4H_2O$ matrix of the dried gels, independent of the dopant and the oxidation state of its precursor, was demonstrated for *Ln* contents up to 30 mol%. Densities of the dried gels were determined and the particle volume shrinkage during the thermal treatment was investigated. X-ray powder diffraction analyses proved the presence of $U_{1-y}Ln_yO_{2\pm x}$ single phase solid solutions for the sintered Nd-doped microspheres and Ce-doped microspheres prepared using the tetravalent precursor. For Ce-doped compositions prepared with the trivalent precursor, the presence of two solid solutions was observed for Ce contents > 15 mol%. The lattice parameters determined for the single phase solid solutions follow Vegard's law and show a decreasing lattice parameter with increasing dopant content. In the case for the Nd-doped material different charge compensation mechanisms, depending on the dopant content, were observed. The conditions applied in this study allow the usage of a solution containing the gelation agents, resulting in a particle fabrication process for the production of Pu and/or minor actinide containing UO_2 transmutation fuel, which has benefits in terms of automating and remote handling, leading to a better implementation in glove boxes or hot cells.

Keywords: nuclear fuel fabrication, co-conversion, sol-gel, internal gelation, GenIV

1. Introduction

The sol-gel route via internal gelation (IG) is a process that is currently explored for the production of minor actinide containing transmutation fuel, which is required for the recycling of spent nuclear fuel, as envisaged by the scientific community for closing the nuclear fuel cycle. The IG process offers the opportunity to convert a solution containing mixtures of different metals into a homogeneous precipitate with a spherical geometry. The advantages of the process are avoidance of handling fine powder and facilitation of automation for the production of nuclear fuel precursors. Those precursors are thermally treated and can be used as particle fuel [1] or compressed into the commonly used fuel pellets [2].

In the context of simulated nuclear fuel materials, lanthanides act commonly as surrogates for actinides. Ce and Nd are used to simulate Pu and Am, respectively. The assignment of the surrogates is based on similar ionic radii [3]. Lundberg and Persson [4] agree to use Nd^{III} (r_{CN9} = 1.161 Å) as surrogate for Am^{III} (r_{CN9} = 1.157 Å) but suggest using Nd^{III} or Pr^{III}

*Corresponding author
Email address: christian.schreinemachers@sckcen.be (Christian Schreinemachers)

(r_{CN9} = 1.176 Å) as replacement for Pu^{III} (r_{CN9} = 1.168 Å), instead of Ce^{III} (r_{CN9} = 1.191 Å). However, one of the most stable plutonium oxidation states is Pu^{IV} (r_{CN8} = 0.97 Å) and Ce as surrogate has the benefit of being used as Ce^{IV} (r_{CN8} = 0.96 Å).

Suresh Kumar et al. [5] tested the IG process for the production of bulk Ce-doped ammonium diuranate (ADU) gels, using Ce^{III} as dopant precursor. Moreover, IG studies to prepare CeO_2 particles are available in literature, they use Ce^{IV} solution, pre-neutralised with NH_3 solution, as metal precursor [6–9]. Katalenich [10] compared the usage of Ce^{III} and Ce^{IV} as metal precursors and came to the conclusion that strong Ce gels with a quick gelation time could be achieved using diammonium cerium(IV) nitrate, whereas a Ce^{III} nitrate feed solution did not lead to satisfying gels.

The gelation process is largely governed by the ratio (R) of the molar amounts of the gelation agents to the molar amounts of the metals. Depending of the metal concentration in the sol, the R value has to be adjusted to ensure proper gelation. A metal concentration of 1.3 mol L^{-1} and a concentration ratio R = 1.2 for both gelation agents was successfully applied for the fabrication of un-doped ADU gels in an earlier study [11]. The parameters are based on the suggestion by Vaidya et al. [12] to form a single phase gel at gelation temperatures of 50 °C to 70 °C. Kumar et al. [13] investigated gelation parameters for the fabrication of $U_{0.47}Pu_{0.53}O_2$ particles and found R values ranging from 1.20 to 1.25 for both gelation agents suitable for a metal concentration of 1.3 mol L^{-1}, which make those conditions promising to introduce a dopant molar metal fraction up to about 50 mol%.

The feasibility of producing Nd-doped UO_2 by internal gelation was successfully demonstrated in an earlier study [14]. In the mentioned study, the sol was prepared by dissolving the solid gelation agents, urea and hexamethylenetetramine (HMTA), in a concentrated metal blend solution ($c(M^{n+})_{sol}$ = 2.5 mol L^{-1}), which was subsequently gelled and thermally treated to form $U_{1-y}Nd_yO_{2\pm x}$ microspheres containing Nd molar metal fractions of up to 43 mol%. The R ratios for urea and HMTA were 1.8 and 1.35 respectively. The process proved successful for microspheres up to elevated Nd dopant levels, but the dissolution of solid gelation agents in the metal solution is a complicated step when envisaging automation.

In the current work, research to further improve the fabrication process of Nd-doped ADU gels, in terms of automating and remote handling, was carried out. The mentioned gelation parameters of R = 1.2 for the gelation agents and a metal concentration of 1.3 mol L^{-1} in the sol were tested. This is a significantly lower metal concentration, compared to the previous study on the fabrication of Nd-doped particles using the IG process ($c(M^{n+})_{sol}$ = 2.5 mol L^{-1}, R_{HMTA} = 1.35, R_{urea} = 1.8) [14], but allows the usage of a solution containing the gelation agents urea and HMTA, instead of dissolving them directly in the sol. The modification has advantages for the particle production in a continuous process, since the R values and the metal concentration in the sol can entirely be controlled by adjusting flow rates of two individual solutions. The impact of this change on the IG process and the final product was studied. Additionally, the gelation parameters were tested to fabricate cerium doped UO_2 particles, using Ce^{III} and Ce^{IV} as dopant precursors.

2. Experimental

2.1. Chemicals

UO_{2+x} (x = 0.06(1)) originated from a stock provided by AREVA and was depleted in $^{235}_{92}U$ (0.3 g / 100 g U). Impurities were analysed and have been found to be < 0.01 wt%. The trivalent lanthanide precursors, $Nd(NO_3)_3{\cdot}6H_2O$ and $Ce(NO_3)_3{\cdot}6H_2O$, were ordered from Strem Chemicals Inc. (≥ 99.9 wt%). Diammonium cerium(IV) nitrate ($(NH_4)_2Ce(NO_3)_6$, for analysis, 99.5 wt%), originated from Acros Organics and nitric acid ($w(HNO_3)$ = 70 wt%; ≥ 99.999 wt%; trace metals basis)

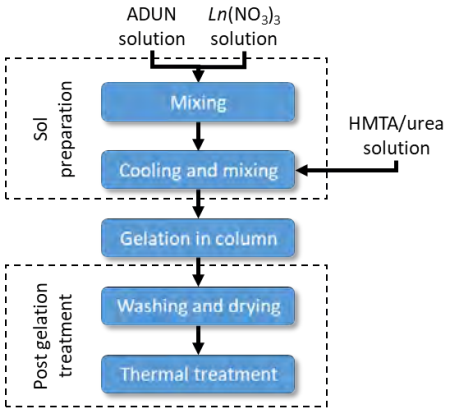

Figure 1: Schematic overview of the IG process, studied to fabricate *Ln*-doped UO_2 microspheres using trivalent *Ln* precursors (*Ln* = Ce and Nd).

was purchased from Aldrich. Ammonia solution ($w(NH_3)$ = 28 wt% to 30 wt%; ACS reagent®), urea (pellets; ≥ 99.5 wt%; ReagentPlus®) and HMTA (≥ 99.0 wt%; ACS reagent®) were ordered from Sigma-Aldrich, while silicone oil (47 V 100) and petroleum benzine (40 °C to 60 °C boiling range; SupraSolv®) originated from VWR.

2.2. *Particle fabrication*

Figure 1 summarises schematically the individual steps of the IG process applied in this study, using an acid-deficient uranyl nitrate (ADUN) solution as uranium precursor. The ADUN solution ($c(U)$ = 2.6 mol L^{-1}, pH = 1.7, ρ = 1.85 g cm^{-3}, $\frac{c(NO_3^-)}{c(U)}$ = 1.56) was fabricated by dissolving β-UO_3 in uranyl nitrate (UN) solution [15]. The preparation of β-UO_3, UN solution, and the ADUN solution is described, amongst others, in our former study [11]. The identical ADUN solution and un-doped particles were used in this work.

2.2.1. *Preparation of un-doped gels*

The ADUN solution (2.0 mL) was stirred in an ice bath and a pre-cooled solution (2.0 mL) containing HMTA (3.1 mol L^{-1}) and urea (3.1 mol L^{-1}) was added, leading to $c(U)$ = 1.3 mol L^{-1} and R = 1.2 for both gelation agents. The sol was dropped manually into a double-walled glass column filled with silicone oil (T = 90 °C) by the use of a syringe and a hollow needle (inner diameter = 0.45 mm). The transfer was carried out in two batches of about 2 mL and the addition of the entire sol took less than 2 min. The fall time of a droplet in the filled column (30 cm height) was about 6 s. When the sol was added, the heating was switched off and the gelled droplets were removed from the column at an oil temperature of 40 °C to perform the post gelation treatment (figure 1). They were washed 3 times with 50 mL of petroleum benzine and stored in 50 mL of ammonia solution ($w(NH_3)$ = 12.5 wt%). After ageing for 24 h, the particles were washed twice with 50 mL of ammonia solution ($w(NH_3)$ = 12.5 wt%) and dried for 24 h at room temperature. Finally, the products were dried at 90 °C and an absolute pressure of 250 mbar for 24 h.

2.2.2. *Preparation of Nd- and Ce-doped gels*

The *Ln* metal fraction $\chi(Ln) = \frac{n(Ln)}{n(U+Ln)}$ was varied from 5 mol% to 30 mol% with an increment of 5 mol%. Hexahydrate nitrates of the trivalent lanthanides and diammonium nitrate of cerium(IV) served as precursors. $Nd(NO_3)_3{\cdot}6H_2O$ and $Ce(NO_3)_3{\cdot}6H_2O$ were each dissolved in ultra pure water and molar metal concentrations of $c(Nd)$ = 2.4 mol L^{-1} and $c(Ce)$ = 2.3 mol L^{-1} were determined via ICP-MS.

The sol was prepared in two steps (sol preparation, figure 1). Firstly, a metal blend solution was prepared by mixing the ADUN solution with the respective volume of the lanthanide nitrate solution. In the case of Ce^{IV} as dopant precursor, $(NH_4)_2Ce(NO_3)_6$ was dissolved directly in diluted ADUN solution to end up with the desired metal ratios. Then, the metal blend solution was cooled in an ice-bath and the pre-cooled solution containing urea and HMTA was added, as described in the previous section. The gelation of the sol and the post gelation treatment were also carried out as described in section 2.2.1. The time between sol addition and gel removal from the column was for all doped compositions about one hour.

2.2.3. Thermal treatment

The gelled particles were calcined in Al_2O_3 crucibles at 900 °C in synthetic air, using a heating rate of 1.5 °C min^{-1} and a holding time of one hour at 900 °C (Nabertherm, LT 9113/P330). The furnace was cooled to 150 °C with a rate of 10 °C min^{-1}, then the crucibles were placed in a desiccator to allow them to cool down to room temperature.

Afterwards, the calcined particles were sintered under reducing conditions in custom made Mo crucibles (Linn High Therm, HT-1800-Moly). Particles of each composition were heated up to 700 °C with 5 °C min^{-1} in Ar atmosphere. Then, the gas atmosphere was changed to Ar:H_2 (95:5) and Ar:O_2 (99.5:0.5) with flow rates of 1428 mL min^{-1} and 72 mL min^{-1}, respectively. Those conditions correspond to an oxygen potential of about −420 kJ mol^{-1}, which is required to prepare undoped, UO_2 at 1600 °C, with a deviation from stoichiometry smaller than 0.0005 [16, 17]. The temperature was held for 2 h at 700 °C before it was further heated to 1600 °C with 5 °C min^{-1}. An isotherm of 10 h was maintained and at its end the atmosphere was switched back to Ar (1500 mL min^{-1}). Then, the samples were cooled down to 200 °C with 5 °C min^{-1} and subsequently placed in a desiccator to reach room temperature.

2.3. Characterisation

All uncertainties in this study are given for a 95 % confidence level (2σ). Where appropriate, the concise notation was used to report uncertainties, where the number in parentheses refers to the last digits of the quoted result.

2.3.1. Determination of U, Nd and Ce concentration

Metal concentrations of the ADUN solution and the trivalent *Ln* precursor solutions were determined via inductive coupled plasma mass spectrometry (ICP-MS). An ELEMENT 2 system (Thermo Scientific) was calibrated with 1 ppb, 2 ppb, 5 ppb, 10 ppb and 20 ppb U, Nd and Ce solutions, prepared from 1000 ppm single element standards (SPEX, CertiPrep) diluted with a matrix consisting of ultrapure water and HNO_3 (2 % $\frac{V}{V}$). A dilution factor of 1:10^8 was applied to the sample solutions. In addition, ICP-MS analyses of the dried gels were performed to determine the actual dopant content of the compositions. Two microspheres of each composition (7.8 mg to 13.7 mg) were dissolved in 1 mL of HNO_3 ($w(HNO_3)$ = 70 wt%), to prepare samples. After dissolution, a volume of 9 mL ultra pure water was added and the solutions were further diluted (1:2000). Moreover, 10 µL of the sol was sampled during the synthesis, which were subsequently mixed with 990 µL of dilution matrix. Those samples were further diluted with a factor of 1:5000. The directly measured mass concentrations have a relative uncertainty of 10 % (2σ) and were converted into the molar concentrations to determine the molar metal fraction of each composition. The propagation of the mass concentrations' uncertainties led to relative molar metal fraction uncertainties (2σ) ranging between 13.7 % (5 % dopant) and 11.1 % (30 mol% dopant).

2.3.2. Optical microscopy (OM)

OM analyses of the dried gels were performed with a HIROX MX-2016Z microscope and a magnification of 100×. Prior to the particle analyses and afterwards, images of a calibration standard were recorded (Keyence OP-88141). A *HI-SCOPE Advanced KH-3000* system (HIROX) was used for the data acquisition, and data processing was done using the software package Fiji (Version 1.52p) [18].

Five particles of each composition were analysed. The individual particle masses were measured during the sample preparation (Mettler-Toledo AT201). Diameters were measured in four positions of each particle (90°, 45°, 0° and −45°), which were averaged and the aspect ratio for each particle was determined ($\frac{d_{max}}{d_{min}}$). Moreover, the average diameter for each individual composition was calculated. Densities were determined, dividing the particle masses by the particle volumes calculated from the diameters, assuming a spherical geometry. The individual densities were also averaged for each composition.

2.3.3. Scanning electron microscopy (SEM)

SEM investigations were carried out to study the shape, morphology and homogeneity of the prepared microspheres, using a Jeol JSM 7100FA field-emission microscope, equipped with a secondary and backscattered electron detector. The working distance ranged from 7 mm to 10 mm and an accelerating voltage of 15 kV was employed. Three sintered particles of each composition were analysed via SEM. The data processing was carried out as described in the previous section for the OM. Diameters and aspect ratios were determined for each particle and average diameters were calculated for the compositions.

2.3.4. X-ray powder diffraction (XRD)

The XRD analyses were carried out using a PANanalytical X'Pert Pro diffractometer. The device utilises a Bragg–Brentano parafocusing geometry in a θ-θ configuration. A sintered, high purity silicon disc was used for zero point calibration. Weekly validations were performed on a sintered alumina disc (NIST Standard Reference Material 1976b). Lattice parameter refinement of silicon was done to asses the instrument bias, which was found to be smaller than 2×10^{-5} relative (2σ). A copper LFF X-ray tube was used as radiation source. The measurement of high-quality diffractograms with low axial divergence was ensured by a combination of a fixed divergence slit, 0.02 rad soller slits and a copper beam mask in the incident beam path.

The sample was mixed with ethanol in a mortar and ground, the resulting suspension was dropped on a zero background silicon single crystal holder. After evaporation of the ethanol, the specimen was mounted into the device and diffractograms were recorded. For the dried gels, a range from 10° to 80° 2θ with a step size of 0.017° 2θ was measured, while the sintered particles were measured in the range from 20° to 143° 2θ, using the same step size.

Lattice parameters were determined using the unit cell refinement option of the software package *HighScore Plus* by PANalaytical (Version 4.8), which applies the method described by Nelson and Riley [19]. For some compositions the presence of two phases was observed, the lattice parameter of those phases were determined applying the Rietveld refinement [20] option of the same software package, details on the approach followed for performing Rieveld refinement are given in section 3.4. Detailed peak shape analyses of the biphasic compositions' reflections were carried out using the application *Fityk* (Version 0.9.8) [21].

3. Results

3.1. Gelation, washing and drying

Nd- and Ce-doped microsphes with *Ln* contents up to 30 mol% were successfully synthesised via internal gelation, using trivalent *Ln* precursors. The actual dopant content in the sol ($\chi(\text{dopant})_{\text{sol}}$, table 1) did not deviate significantly from the aimed content ($\chi(\text{dopant})_{\text{aimed}}$, table 1). Intact spheres were obtained and the spherical shape remained during the washing, ageing and drying steps. No broken particles were observed for any of the compositions.

Table 1: Dopant molar metal fractions determined via ICP-MS in the sol ($\chi(\text{dopant})_{\text{sol}}$) and for dissolved particles ($\chi(\text{dopant})_{\text{particle}}$), as well as diameters of the dried particles (d_{dried}, OM) and sintered particles (d_{sintered}, SEM), including the largest aspect ratio of each batch.

dopant precursor	$\chi(\text{dopant})_{\text{aimed}}$ / mol%	$\chi(\text{dopant})_{\text{sol}}$ / mol%	$\chi(\text{dopant})_{\text{particle}}$ / mol%	d_{dried} / mm	aspect ratio	d_{sintered} / mm	aspect ratio
–	0			1.51(3)	1.04	0.78(5)	1.01
Nd^{III}	5	5.2(7)	5.3(7)	1.57(2)	1.03	0.78(3)	1.01
	10	[a]	11(1)	1.54(2)	1.03	0.77(1)	1.01
	15	16(2)	16(2)	1.89(4)	1.02	0.89(2)	1.02
	20	20(2)	22(3)	1.58(7)	1.04	0.86(1)	1.01
	25	26(3)	25(3)	1.79(8)	1.07	0.96(6)	1.02
	30	31(3)	30(3)	1.59(2)	1.03	0.93(7)	1.02
Ce^{III}	5	5.1(7)	5.1(7)	1.36(3)	1.02	0.75(5)	1.01
	10	10(1)	10(1)	1.39(2)	1.01	0.78(4)	1.01
	15	15(2)	16(2)	1.37(6)	1.02	0.77(5)	1.01
	20	20(3)	21(3)	1.34(7)	1.05	0.78(1)	1.01
	25	26(3)	25(3)	1.57(4)	1.02	0.90(1)	1.01
	30	32(4)	31(3)	1.53(3)	1.04	[b]	
Ce^{IV}	5	4.7(6)	4.8(7)	1.30(2)	1.02	0.88(4)	1.01
	10	10(1)	10(1)	1.28(2)	1.12	0.88(5)	1.02
	15	14(2)	14(2)	[c]			
	20	20(2)	20(2)	[c]			

[a] Not analysed, since a mistake occurred during the sampling of the sol.

[b] No diameters determined, since particles broke apart during sintering.

[c] No diameters determined, since no spherical geometry was obtained.

In the case of Ce^{IV} as *Ln* precursor, an incomplete gelation was observed for compositions with ≥ 10 mol% Ce, resulting in a minor fraction of agglomerated spheres for a Ce content of 10 mol%. For the compositions with Ce contents of 15 mol% and 20 mol% no spherical shape could be obtained using the chosen gelation parameters. Therefore it was decided to not further increase the Ce content for this precursor.

The Nd-doped gels shrunk significantly during the drying at room temperature, but no remarkable observations were made during the washing of those particles. However, the Ce-doped gels prepared with Ce^{III} changed their colour from yellow to a bright shade of green during the ageing in NH_3 solution. For the Ce-doped compositions prepared with the Ce^{IV} precursor, this colour change did not occur during the washing steps, but while drying in air the particles turned into dark-green.

The smallest batch mass of gels prior to the drying at 90 °C and 250 mbar was found for the 30 mol% Nd-doped composition (1.21 g), while the largest batch mass occurred for the 20 mol% Ce-doped composition (Ce^{IV} precursor, 1.95 g). The individual masses are listed in the dataset of this study [22].

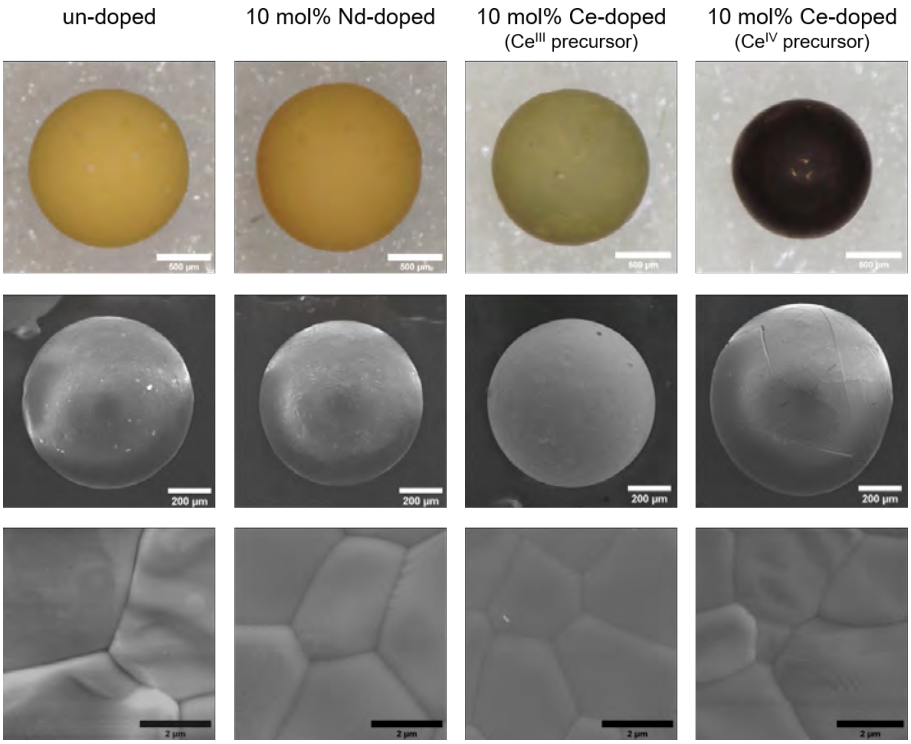

Figure 2: Micrographs of a dried un-doped microsphere and dried microspheres doped with 10 mol% Nd and 10 mol% Ce recorded via OM (top), as well as SEM micrographs of the particles after sintering (middle), and close-ups of the sintered particles' surface (bottom).

3.2. Characterisation of dried gels

The dopant molar metal fractions determined in the dried particles ($\chi(\text{dopant})_{\text{particles}}$, table 1) are in good agreement to the aimed contents ($\chi(\text{dopant})_{\text{aimed}}$, table 1). Representative micrographs of a dried, un-doped particle and dried particles doped with 10 mol% Nd and 10 mol% Ce, recorded via OM, are presented in figure 2 (top). Images of 5 particles per composition were used to determine particle diameters, which were found to range between 1.28(2) mm and 1.89(4) mm for the individual compositions, the results are listed in table 1. The largest aspect ratios of the individual compositions varied between 1.01 and 1.07 (table 1). For the composition doped with 10 mol% Ce (Ce^{IV} precursor), a higher aspect ratio was observed (1.12).

Densities of the dried particles, determined by OM, are presented in figure 3. The plot also contains the as yet unpublished data of Nd-doped gels, prepared with different metal concentrations and gelation agent rations: $c(M^{n+})_{\text{sol}} = 2.5\,\text{mol}\,\text{L}^{-1}$, $R_{\text{HMTA}} = 1.35$, $R_{\text{urea}} = 1.8$ [23], which were determined in a similar way via OM.

A comparison of the densities obtained for the dried, Nd-doped gels, reveals a significant difference for the two gelation conditions. The densities of the Nd-doped gels prepared within this study ($c(M^{n+})_{\text{sol}} = 1.3\,\text{mol}\,\text{L}^{-1}$, $R_{\text{HMTA}} = R_{\text{urea}} = 1.2$) are ranging between $1.87\,\text{g}\,\text{cm}^{-3}$ and $2.62\,\text{g}\,\text{cm}^{-3}$, with an outlier for the 15 mol% Nd-doped composition ($1.57\,\text{g}\,\text{cm}^{-3}$). The density obtained for the un-doped gel ($1.95\,\text{g}\,\text{cm}^{-3}$) was found to be in the same range than those of the gels with Nd contents ≤ 10 mol%. For Nd contents of 20 mol% and 25 mol%, an increased density was observed ($2.17\,\text{g}\,\text{cm}^{-3}$ and $2.18\,\text{g}\,\text{cm}^{-3}$). The highest density of this batch ($2.62\,\text{g}\,\text{cm}^{-3}$) was found for the 30 mol% Nd-doped composition. For the particles prepared with a higher metal concentration in the sol ($c(M^{n+})_{\text{sol}} = 2.5\,\text{mol}\,\text{L}^{-1}$, $R_{\text{HMTA}} = 1.35$, $R_{\text{urea}} = 1.8$) [23], a smaller density variation for a larger dopant range was observed, the maximum Nd content corresponds to 42.63 mol%. The densities of those compositions varied between $4.15\,\text{g}\,\text{cm}^{-3}$ and $3.81\,\text{g}\,\text{cm}^{-3}$, and a decreasing density with increasing Nd content was observed.

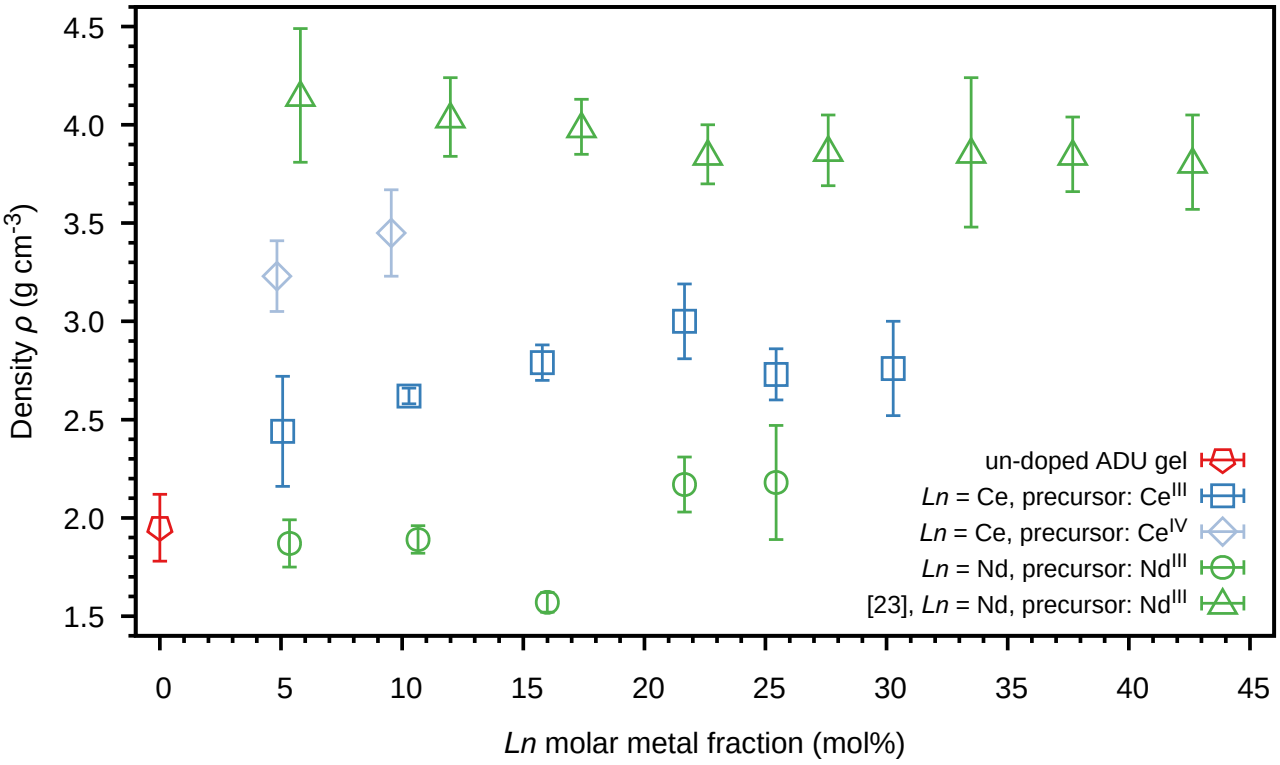

Figure 3: Densities of dried un-doped gels, and dried gels doped with Nd and Ce, prepared using $c(M^{n+}) = 1.3\,\mathrm{mol\,L^{-1}}$, $R_{\mathrm{HMTA}} = R_{\mathrm{urea}} = 1.2$, as well as densities of dried Nd-doped gels prepared using different gelation parameters ($c(M^{n+}) = 2.5\,\mathrm{mol\,L^{-1}}$, $R_{\mathrm{HMTA}} = 1.35$, $R_{\mathrm{urea}} = 1.8$) [23].

The densities of the dried, Ce-doped gels are ranging between the densities determined for the Nd-doped compositions (figure 3). For the compositions prepared with the Ce^{III} precursor, a density of $2.44\,\mathrm{g\,cm^{-3}}$ was found for the 5 mol% doped composition. The density increased with increasing Ce content, reaching a maximum of $3.00\,\mathrm{g\,cm^{-3}}$ for the compositions containing 20 mol% Ce. For Ce contents of 25 mol% and 30 mol%, a comparable density of $2.73\,\mathrm{g\,cm^{-3}}$ and $2.76\,\mathrm{g\,cm^{-3}}$ was determined.

The usage of the Ce^{IV} precursor led to gels with a higher density than those prepared with Ce^{III} (figure 3). Values of $3.23\,\mathrm{g\,cm^{-3}}$ and $3.45\,\mathrm{g\,cm^{-3}}$ were determined for the 5 mol% and 10 mol% Ce-doped compositions, respectively. Since only those compositions could be fabricated maintaining a spherical shape, only two data-points for this series are included in the plot.

Figure 4 shows the XRD pattern obtained for the dried un-doped microspheres (also published in [24]) (a), and the dried gels doped with Nd (b) and Ce (c). For both dopants the compositions with 10 mol% molar metal fraction are exemplarily shown, the XRD pattern of the dried compositions for the entire dopant range are part of the dataset of this study [22]. The un-doped material was identified as ADU with $3UO_3{\cdot}2NH_3{\cdot}4H_2O$ stoichiometry [11] and its diffractogram looks, apart from obvious intensity variations, comparable to one of the 10 mol% Nd-doped composition (figure 4b). The shoulder of the reflection at 25.25° 2θ is more emphasised, but no additional reflections occur compared to the un-doped material. The XRD patterns of the Ce-doped compositions (figure 4c) show a significantly different degree of crystallinity for the different Ce precursors. For Ce^{III} comparable XRD patterns to those obtained for the Nd-doped particles were observed, whereas the XRD pattern of the compositions prepared with Ce^{IV} show a remarkably lower peak-to-background ratio, indicating large fractions

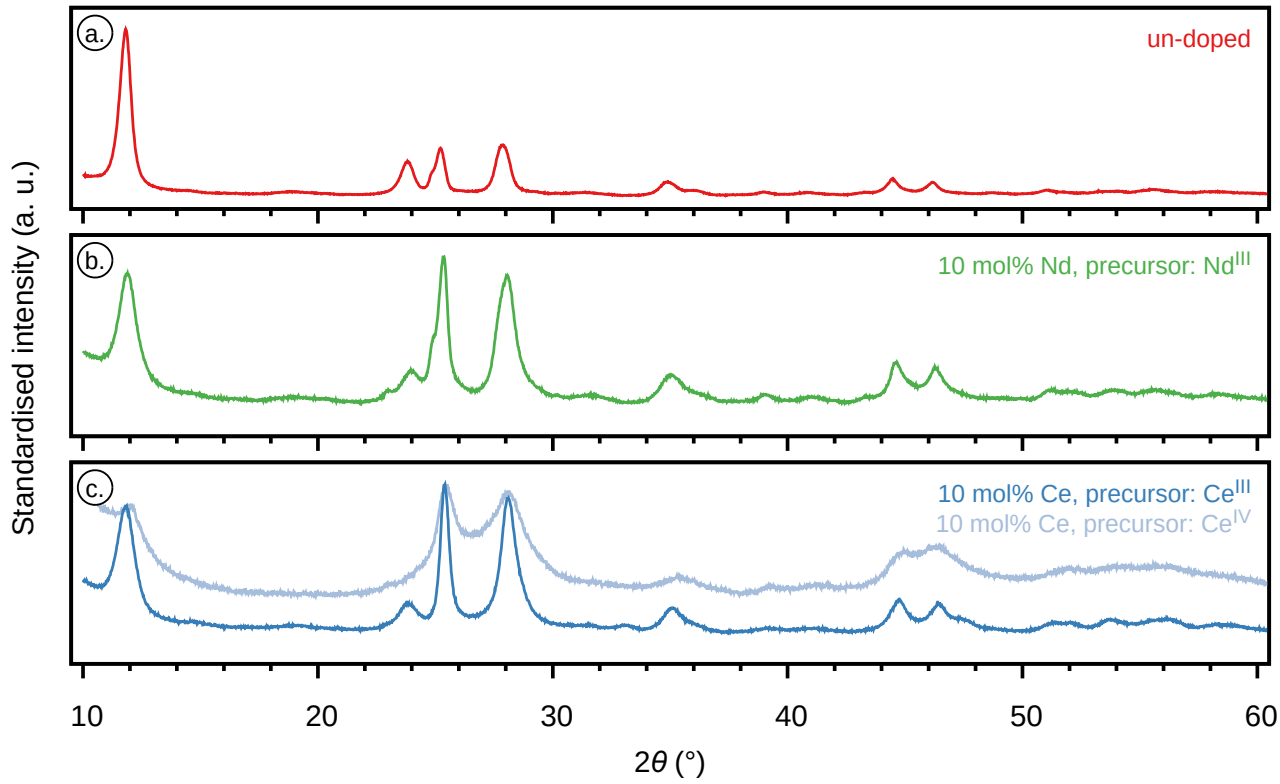

Figure 4: XRD pattern obtained for the dried un-doped gel (a.) [24] and gels doped with 10 mol% Nd (b.) and 10 mol% Ce (c.), prior to the thermal treatment.

of an amorphous phase. For all Ce-doped compositions no additional reflections compared to the un-doped material can be observed. A close inspection of the diffractograms (see also [22]) reveals a shift of the reflections to higher 2θ angles with increasing dopant content for both dopants, indicating a lattice contraction that might be caused by the incorporation of the dopant into the ADU matrix.

3.3. Thermal treatment

The particles' spherical shape for all compositions, prepared using the trivalent *Ln* precursors, was maintained during the calcination at 900 °C in air and no broken microspheres were observed. Moreover, no significant shrinkage of the particles took place within the treatment.

During the sintering in reducing conditions at 1600 °C for 10 h, the un-doped particles and all Nd-doped particles remained in their spherical shape. For the compositions containing 20 mol% and 25 mol% Ce (Ce^{III} precursor), a remarkable fraction of broken particles was observed, while for the 30 mol% Ce composition only a negligible amount of spheres was retained. All compositions underwent a significant shrinkage within this step, which is further elaborated in the discussion section.

3.4. Characterisation of final products

Representative SEM micrographs of un-doped and 10 mol% *Ln*-doped microspheres are shown in figure 2 (middle). Diameters of the microspheres were measured and ranged between 750(50) µm and 960(60) µm for the individual compositions. The aspect ratio was found to be between 1.01 and 1.02, proving the spherical shape of the microspheres. The results of those calculations are included for the individual batches in table 1. However, for the Ce-doped particles prepared with the Ce^{IV}

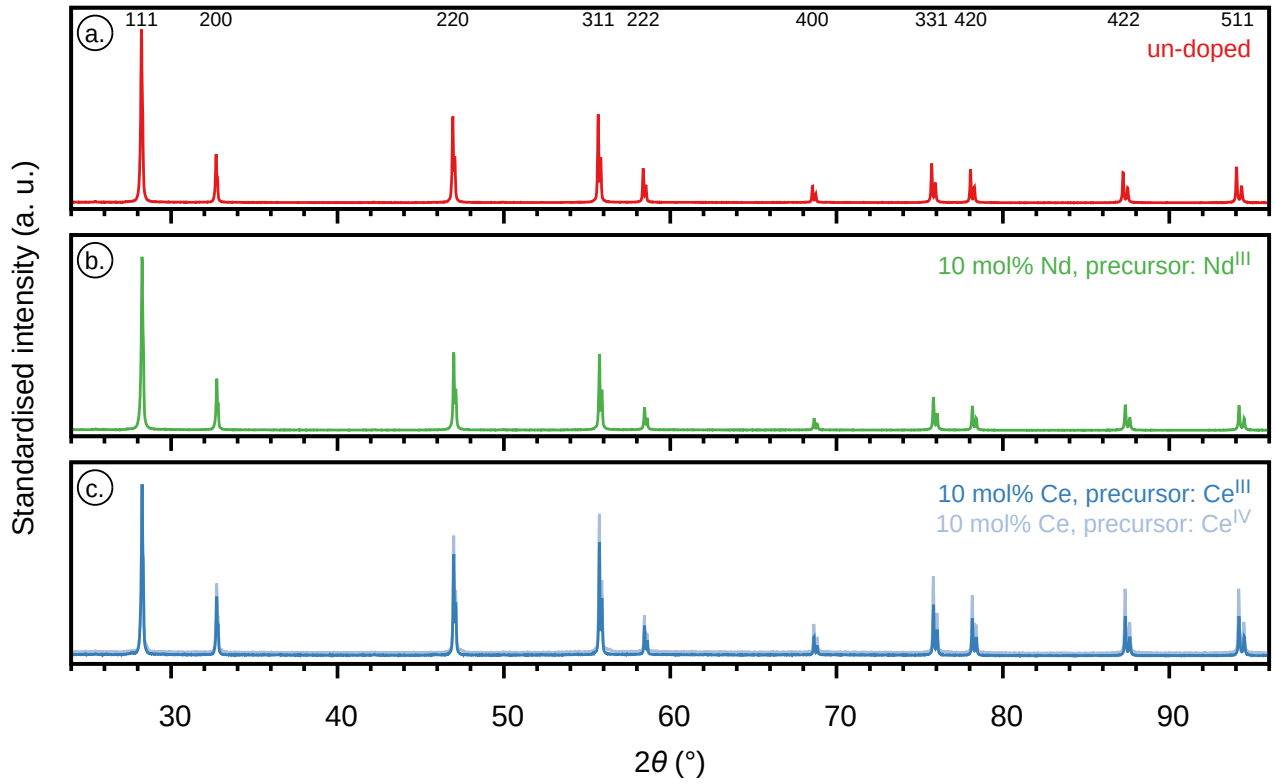

Figure 5: XRD pattern obtained for un-doped UO_2 microspheres (a.) and products doped with 10 mol% Nd (b.) and 10 mol% Ce (c.), as well as the corresponding Miller indices.

precursor, a large amount of cracks on the particles' surface was observed, which was not the case for the particles prepared using Ce^{III}. Close-ups of the surfaces (figure 2, bottom) show grains with neither intergrain nor intragrain pores in the material.

Figure 5 illustrates the XRD pattern of the sintered un-doped microspheres (a.) and exemplarily those of the 10 mol% doped particles. The XRD pattern of the sintered particles for both dopants and the entire dopant range are part of the dataset of this study [22]. The XRD data were used to determine lattice parameters for the individual compositions. The Cu $K\alpha_1$ wavelength of 1.540 592 9 Å [25] was used, and a small correction for the temperature difference of the actual acquisition temperature with respect to a reference value of 20 °C was applied [17]. For the latter, the thermal expansion coefficient published for UO_2 by Fink [26] was used. The results are plotted as function of the *Ln* molar metal fraction in figure 6.

Two different linear trends, depending on the dopant content, were observed for the Nd-doped compositions. The slope of the linear function was determined by a linear fit constrained at 0 mol% dopant level to intercept with the lattice parameter of stoichiometric UO_2 at 20 °C (5.4713(2) Å) [17]. A slope of $-6.57(13) \times 10^{-4}$ with a correlation of 0.949 was determined for Nd contents of ≤ 10 mol%. The slope for compositions with Nd contents of ≥ 15 mol% was determined in the same way and was found to be $-5.24(4) \times 10^{-4}$ ($R^2 = 0.976$).

Detailed analyses of the diffractograms revealed that the Ce-doped samples prepared using the Ce^{III} precursor with Ce contents above 15 mol% are not monophasic. A magnification of the (026) reflection is exemplarily shown in figure 7 for the compositions containing ≥ 15 mol% Ce (Ce^{III} precursor). In the case of the 15 mol% Ce-doped composition, this reflection could be fitted with a *Pseudo-Voigt* function for each of the $K\alpha_1$ and $K\alpha_2$ peaks (figure 7a), leading to the red line which describes the experimental data points very well. For the compositions with ≥ 20 mol% Ce, two further *Pseudo-Voigt* functions

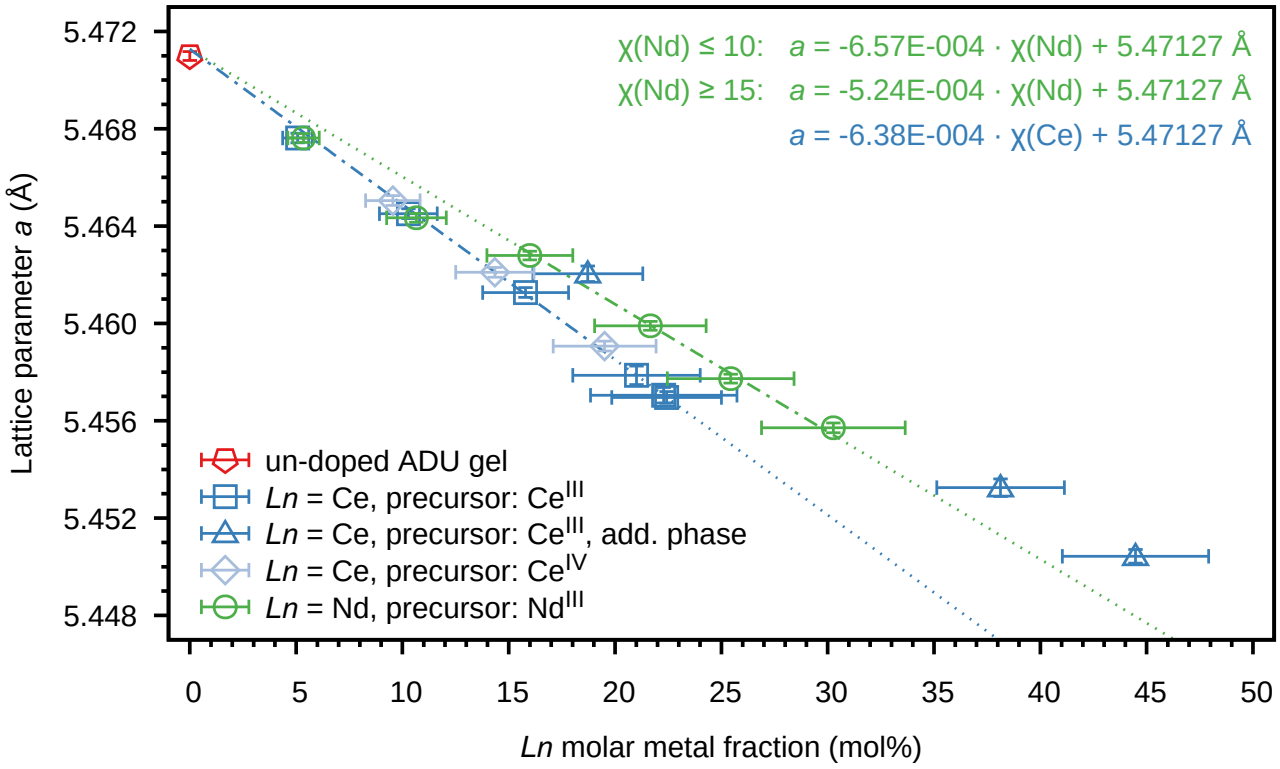

Figure 6: Lattice parameter a as function of the Ln molar metal fraction of the sintered microspheres for Ln = Nd and Ce, prepared using Nd^{III}, Ce^{III} and Ce^{IV} precursors, as well as linear fits forced through an intercept corresponding to the lattice parameter of stoichiometric UO_2 [17]. The uncertainties are given with a confidence level of 2σ.

(orange lines) had to be introduced (figure 7b-d), leading to sums (black lines) which match the experimental data points and indicate that those compositions are biphasic. In order to quantify the weight fractions corresponding to each phase, Rietveld refinements were performed with the following assumptions: (1) two $U_{1-y}Ce_yO_2$ phases are considered, both assuming a fluorite structure ($Fm\bar{3}m$), (2) the Ce content y in each phase is fixed at the nominally aimed molar metal fraction, i. e. 0.20, 0.25, 0.30. One might expect to have different Ce contents in both phases, however, the effect on the diffracted intensity is only marginal even when an uncertainty interval in the order of ±0.1 is considered. Since the Rietveld refinement is not measurably affected when varying the actual Ce content, it was preferred to keep the compositions constrained to their nominal Ce content for the refinement process. Moreover, the Rietveld refinement was restricted to the range 83° to 143° 2θ to minimise the possible divergence caused by the sample preparation method used for XRD (i.e. pipetting of a suspension on a zero-background holder can induce some degree of preferential orientation). Additionally, the high-angle region is most sensitive to probing peak shifts due to variations in lattice parameter, and satisfying *goodness of fit* factors were obtained (2.2 % to 2.5 %). The refinement parameter set consisted of a cubic Chebyshev polynomial to model the background, the scale factor and lattice parameter of both phases along with a global parameter for sample displacement, and two Pseudo Voigt profile functions.

The Rietveld refinement revealed for all affected compositions a majority phase (64 wt% to 75 wt%) having similar lattice parameters (5.4570(2) Å, 5.4579(4) Å and 5.4570(3) Å), indicating a solubility limit for Ce incorporation under the applied conditions. Based on the lattice parameters, the expected Ce content was calculated using the linear relation found for the single phase Ce-doped samples ($\frac{da}{dy} = -6.38(7) \times 10^{-4}$, $R^2 = 0.908$, figure 6). Ce molar metal fractions of 22.4 mol%,

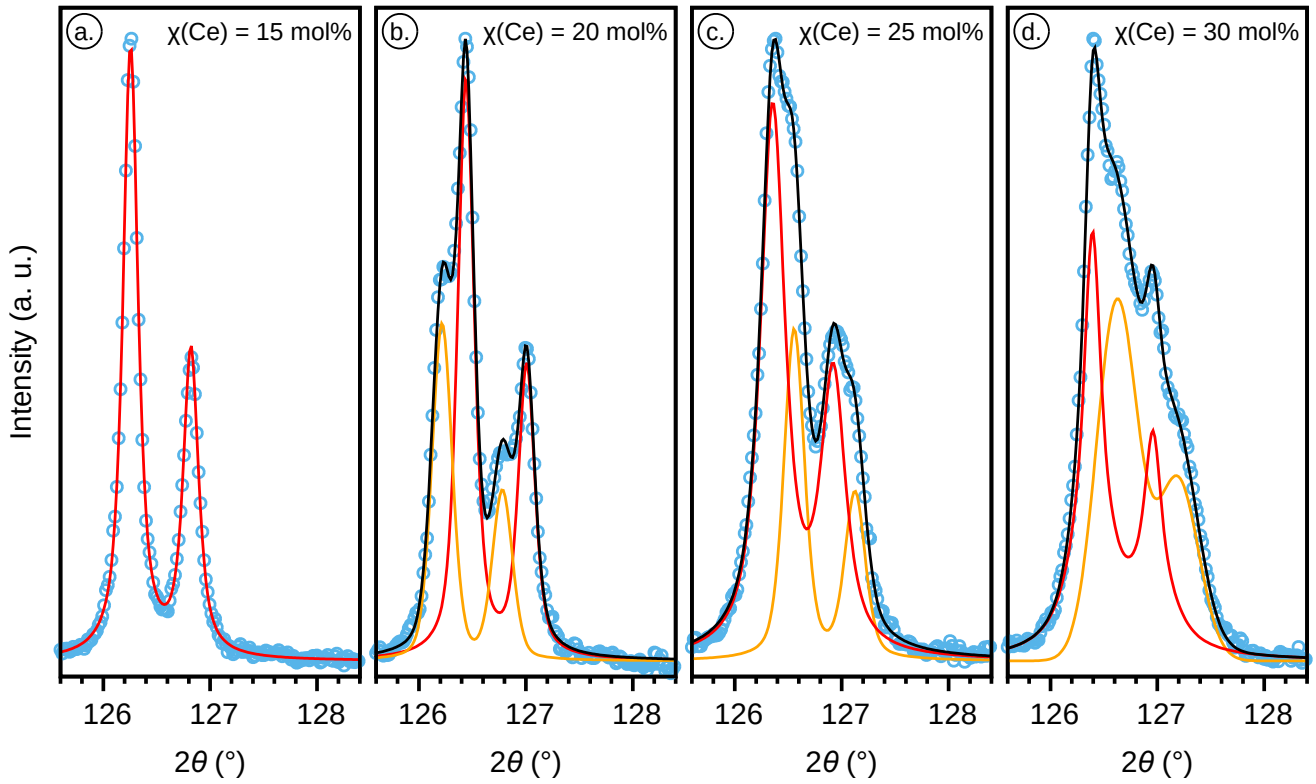

Figure 7: Background subtracted experimental XRD data of the sintered microspheres with Ce contents ≥ 15 mol%, prepared using Ce^{III}, for the 2θ range from 125.6° to 128.4° (reflection with *hkl* equals 026), as well as *Pseudo-Voigt* fits for the majority phase (red), the additional phase (orange) and their sum (black).

21.0 mol% and 22.3 mol% were determined. From those values, the known total Ce-content ($\chi(\text{dopant})_{\text{particle}}$, table 1), and the weight fraction attributed to each phase, the Ce content in the additional phase can be derived. The lattice parameters of the additional phases (5.4620(3) Å, 5.4532(4) Å and 5.4504(3) Å) are plotted as function of the resulting Ce molar metal fractions (18.7 mol%, 38.1 mol% and 44.5 mol%) in figure 6 as well. They seem to have a linear relation with a slightly larger slope than the one observed for the Nd-doped compositions with Nd contents ≥ 15 mol%, which is further discussed in section 4.3.

4. Discussion

4.1. Gelation process and properties of dried gels

During the ageing and washing of the gelled droplets with ammonia solution, some erosion was visually observed. Similar observations were made by Hunt et al. [27] for ADU gels fabricated with different sol compositions but at comparable temperatures. The ICP-MS analyses of the dissolved particles revealed for all *Ln*-doped compositions a relative deviation between the actual dopant content ($\chi(\text{dopant})_{\text{particle}}$, table 1) and the aimed dopant content of ≤ 8.5 %. The largest differences occurred for the Nd-doped compositions with Nd contents up to 20 mol% (6.7 % to 8.5 %). For the Ce-doped compounds prepared with Ce^{III}, the relative differences ranged between 2 % and 5.5 %, while it was ≤ 4 % for the compounds prepared using the Ce^{IV} precursor. The dopant molar metal fractions determined in samples of the sol ($\chi(\text{dopant})_{\text{sol}}$, table 1) exhibit slightly different variations from the aimed dopant content compared to the contents determined in the dissolved particles ($\chi(\text{dopant})_{\text{particle}}$, table 1). However, all observed deviations are within the molar metal fractions' uncertainty, allowing us to conclude that no remarkable leaching effect on one of the metals occurred during the washing and ageing steps of the IG synthesis process.

The incomplete gelation observed for the compositions prepared with the Ce^{IV} dopant precursor might be explained by the fact that a sol containing the Ce^{IV} precursor has a lower initial pH compared to a sol containing the Ce^{III} precursor. The pH difference between the initial pH and the pH of the component precipitating at the highest pH value defines the amount of NH_3 needed to ensure a complete gelation. Thus, the incomplete gelation can be prevented by an increase in HMTA to generate more NH_4^+ ions during the gelation, or by performing a pre-neutralisation of the sol with NH_3 solution like it was done for the synthesis of pure CeO_2 particles (e.g. $\frac{n(OH^-)}{n(Ce)} = 0.5$ [7]). Since we gel mixtures of metals, the latter approach might lead to a precipitation of one of the metals already within the sol preparation step, which will adversely affect the product homogeneity. Moreover, it adds complexity to the synthesis process, which is a disadvantage in terms of remote handling and automation. A better approach would be to investigate the effect of different R values and/or metal concentrations on the gelation process.

The conditions we applied during the gelation are comparable to those applied by Kumar et al. [13] for the fabrication of $U_{0.47}Pu_{0.53}O_2$ microspheres. The sol contained analogous amounts of metals and gelation agents, and similar temperatures were applied during the gelation. Kumar et al. [13] did not describe the speciation of the Pu in their sol, but mentioned that they used different Pu precursor solutions with $\frac{n(NO_3^-)}{n(Pu)}$ ratios of 2.98 to 4.10, allowing us to conclude that the Pu was present in its trivalent and tetravalent oxidation state. The applied gelation parameters led to intact sperically shaped gels for the dopants Ce and Pu using the trivalent precursors. If the different dopant levels are neglected, the results imply that Ce^{III} resembles Pu^{III} and is a suitable substitute for trivalent Pu during the wet chemistry steps. For the tetravalent precursors, our results are not transferable to the study of Kumar et al. [13]. A consequence of diammonium cerium nitrate as precursor is a $\frac{n(NO_3^-)}{n(Ce)}$ ratio of 6, which causes a small lower pH and might adversely affect the stability of the sol due to a more likely protonation of HMTA compared to smaller $\frac{n(NO_3^-)}{n(M)}$ ratios [28]. However, this should result in a premature gelation and not in an incomplete gelation as observed by us, underlining the assumption that the amount of HMTA has to be increased to gel mixtures of uranyl and tetravalent cerium.

4.2. Thermal treatment

During the thermal treatment, a significant shrinkage of the microspheres was observed. Figure 8 shows the ratios of the dried particles' volume and the sintered particles' volume. The volumes were calculated using the diameters determined via OM for the dried particles and by SEM for the sintered particles. Additionally, a data series for the Nd-doped gels [23], prepared with $c(M^{n+})_{sol} = 2.5\,mol\,L^{-1}$, $R_{HMTA} = 1.35$, $R_{urea} = 1.8$, is included in the plot.

We can observe significant shrinkage variations for the different compounds prepared within this study. The volume of the dried, un-doped particles was found to be 7.55 times higher than the volume of the sintered, un-doped particles. For compounds doped with up to 15 mol% Nd, a decrease in volume in the range of 8 to 9 was observed during the thermal treatment, while higher Nd contents resulted in less shrinkage. The compositions doped with 20 mol% and 25 mol% Nd showed a volume loss of a factor of about 6.2, and in the case for the 30 mol% Nd-doped compositions it was about 5. The Ce-doped compositions prepared with Ce^{III} decreased in volume in the range of 5 to 6 during the thermal treatment, while the compositions prepared using Ce^{IV} showed a shrinkage factor of about 3.1. Despite the high shrinkage ratios, a good sphericity was maintained in the Nd-doped particles (table 1), while the less significant shrinkage in the Ce-doped particles (Ce^{III} precursor) resulted in a large fraction of broken particles for higher dopant contents. This might be related to the occurrence of both, trivalent and tetravalent cerium [29], whereas neodymium is known to not change its oxidation state.

The volume shrinkage factors, determined for the Nd-doped microspheres from Schreinemachers [23], are notably smaller

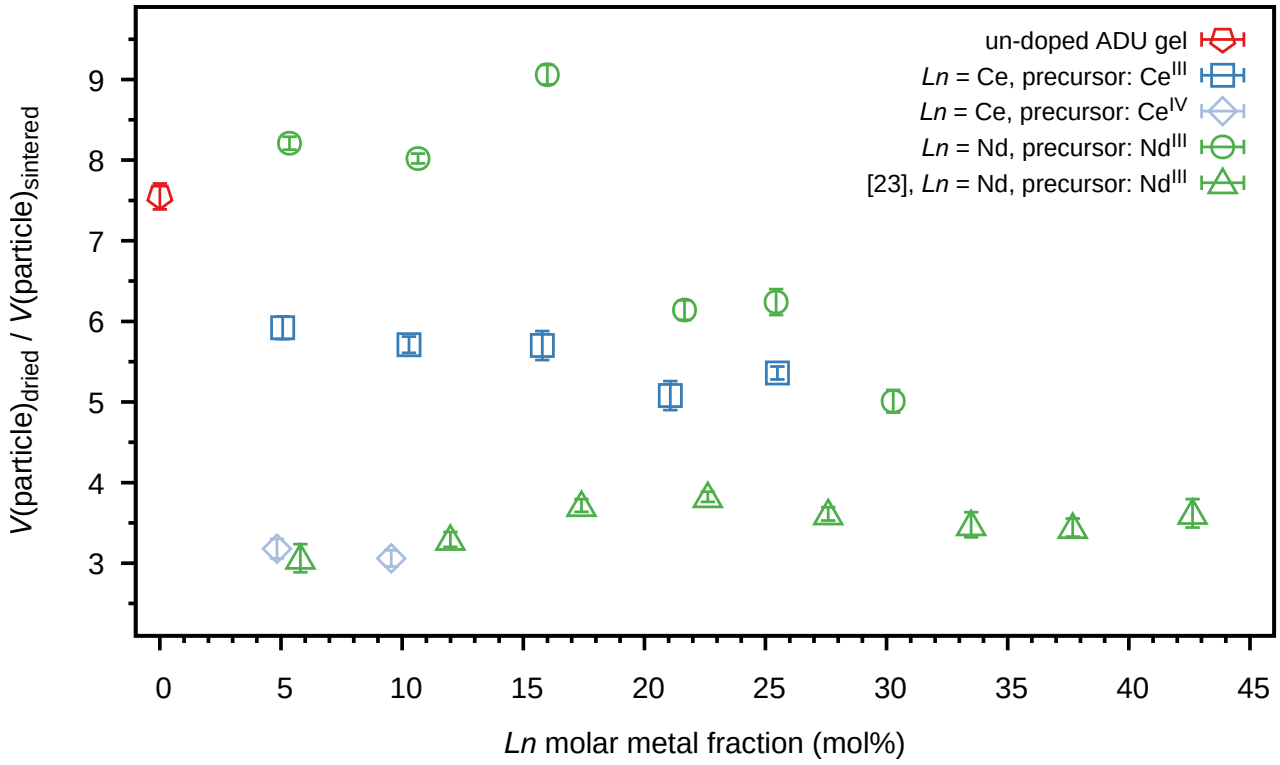

Figure 8: Volume of dried particles (derived from OM) standardised to volume of sintered particles (derived from SEM). Data for un-doped microspheres, and microspheres doped with Nd and Ce, prepared using $c(M^{n+}) = 1.3\,\mathrm{mol\,L^{-1}}$, $R_{\mathrm{HMTA}} = R_{\mathrm{urea}} = 1.2$, as well as data for Nd-doped microspheres prepared using different gelation parameters ($c(M^{n+}) = 2.5\,\mathrm{mol\,L^{-1}}$, $R_{\mathrm{HMTA}} = 1.35$, $R_{\mathrm{urea}} = 1.8$) [23]. The uncertainties are given with a confidence level of 2σ.

than those observed in this study. Volume ratios between 3.06 and 3.82 where observed, which are in the range of those we determined for the Ce-doped particles prepared with Ce^{IV}. Even though a lower sintering temperature was applied in the earlier work (1300 °C, 2 h) [23], we assume the difference is a consequence of the lower metal concentration used in our study.

4.3. Lattice parameter

A lattice parameter of 5.4710(2) Å was determined for the un-doped material at 20 °C. The result is marginally smaller, than the UO_2 lattice parameter published by Leinders et al. [17] (5.4713(2) Å at 20 °C), but the uncertainty intervals overlap, allowing us to conclude that the material represents a pure UO_2 phase.

A comparison of the lattice parameters obtained for the Nd-doped material, along with data reported in literature, is presented in figure 9. As mentioned in the results section, we observed a slope of $-6.57(13) \times 10^{-4}$ for the compositions with Nd contents of < 15 mol% (dashed line, figure 9), and a slope of $-5.24(4) \times 10^{-4}$ for Nd contents between 15 mol% and 30 mol% (dashdotted line, figure 9). Those trends reflect the findings of Bès et al. [30], who described different charge compensation mechanisms in $U_{1-y}Nd_yO_2$ solid solutions, depending on the Nd content. For $y < 0.2$ the formation of U^{5+} was observed, while the formation of U^{5+}, U^{6+} and oxygen vacancies took place for $0.2 \leq y \leq 0.6$, and for $y > 0.6$ the formation of U^{6+} dominated. The occurrence of different charge compensation mechanisms influences the lattice parameter evolution as a function of dopant content, as our data demonstrate.

Interestingly, lattice parameters of a composition doped with 27 mol% Nd (Une and Oguma [31]) and 40 mol% Nd (Wadier [32]) show a comparable trend to the fit of our samples with Nd contents < 15 mol%. The fit obtained for our samples with Nd

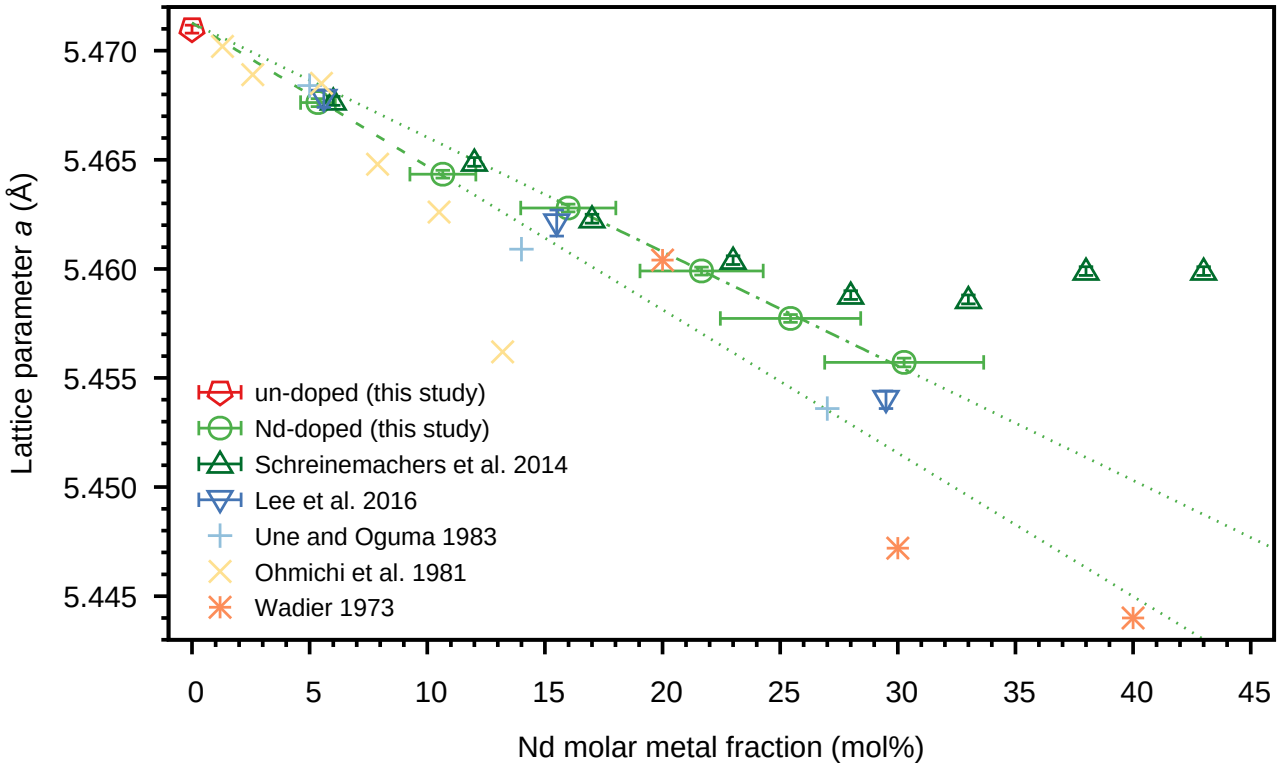

Figure 9: Lattice parameter a as function of the Nd molar metal fraction of the sintered, Nd-doped microspheres, compared to literature data [14, 31–34]. The uncertainties are given with a confidence level of 2σ.

contents between 15 mol% and 30 mol% matches well to the lattice parameter of a 20 mol% Nd-doped composition (Wadier [32]), which is in agreement to the findings of Bès et al. [30], but a comparable trend was also found for a 5.5 mol% Nd-doped compositions (Ohmichi et al. [33]), which can be explained by a hypo-stoichiometric composition of their sample ($\frac{O}{M}$ = 1.9744). A comparison of the reference data, reveals another linear dependency for 1.29 mol%, 2.58 mol%, 7.89 mol% and 10.5 mol% Nd-doped compounds investigated by Ohmichi et al. [33] and a 30 mol% Nd-doped composition of Wadier [32]. Lee et al. [34] published lattice parameters for 5.6 mol%, 15.5 mol%, 29.5 mol% and 53 mol% Nd-doped UO_2. The data for $\frac{O}{M}$ = 2 are included in figure 9 and show a linear dependency with a good correlation of the 5 mol% Nd-doped compound of Une and Oguma [31]. Their linear fit is in between of the two functions determined for the Nd-doped compounds of this study.

The lattice parameter of the 5.80 mol% Nd-doped composition (5.4677 Å), prepared via IG with a higher metal concentration in the sol [14], is comparable to the one of the 5 mol% Nd containing sample from this study. The samples with 11.99 mol% and 17.40 mol% Nd, of the earlier study [14], match the trend observed for the compositions containing $<$ 15 mol% of the current study, while a comparable lattice parameter ranging between 5.4586 Å and 5.4604 Å for the compositions with Nd contents $\geq$ 22.62 mol% from the earlier study indicate that no solid solution was formed in those compounds, which was not the case for the Nd-doped particles of this work.

A comparison of the lattice parameter obtained for the Ce-doped material is presented in figure 10. The single phase Ce-doped compositions show a linear behaviour with a slope of $-6.38(7) \times 10^{-4}$ (R^2 = 0.908). The experimental lattice parameters of this study for Ce dopant contents below the solubility limit of 22.4 mol% agree well to reference data [35–

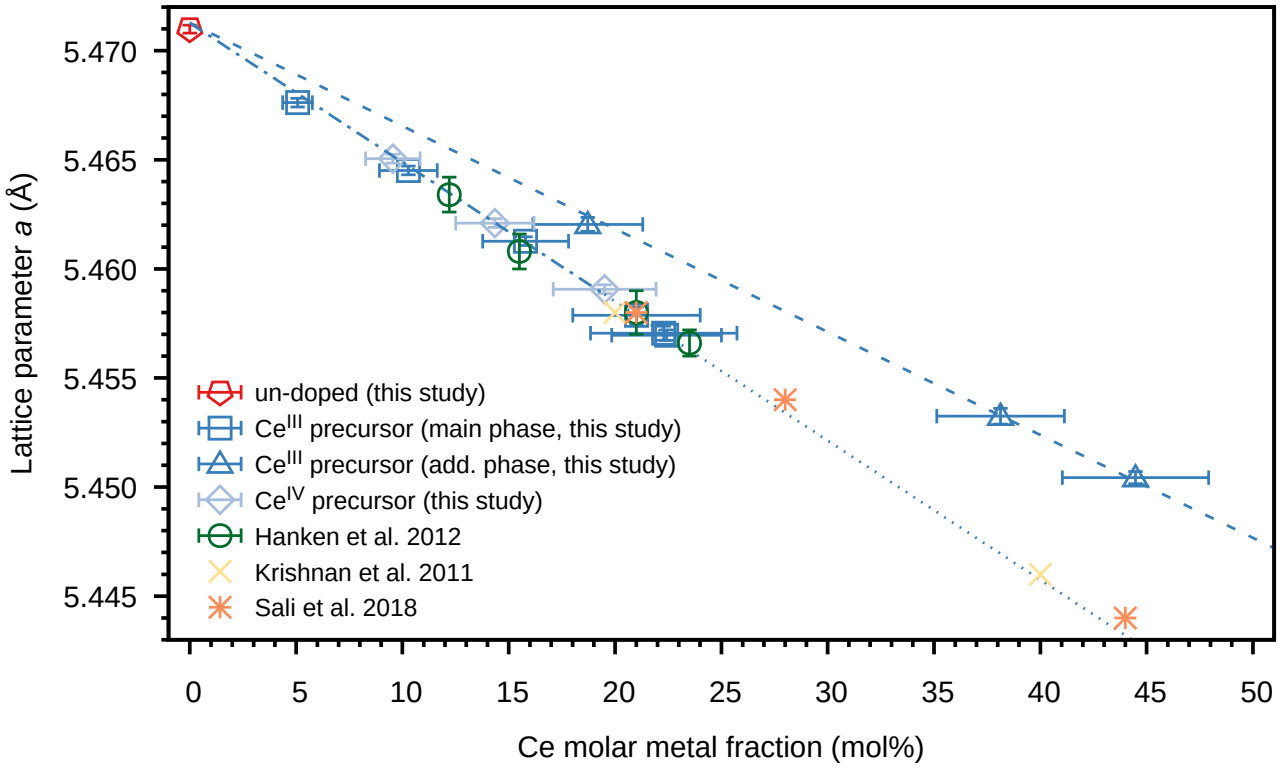

Figure 10: Lattice parameter a as function of the Ce molar metal fraction of the sintered, Ce-doped microspheres, compared to literature data [35–37]. The uncertainties are given with a confidence level of 2σ.

37] (figure 10). The reference material was prepared by solid-state synthesis and co-precipitation [35], but also a citrate combustion method [36, 37] was applied. The obtained powders were pelletised and sintered in Ar/H_2 mixtures with H_2 contents of 5 % or 8 %, equilibrated with water (O_2 potential: $-416\,\mathrm{kJ\,mol^{-1}}$ to $-347\,\mathrm{kJ\,mol^{-1}}$), the sintering temperatures ranged between 800 °C and 1450 °C. Even though a remarkably lower sintering temperature was applied, Venkata Krishnan et al. [36] and Sali et al. [37] obtained single phase solid solutions for compositions with Ce contents > 22.4 mol%, following the trend we observed for the majority phase in our samples.

The additional phase, present in the biphasic compositions, depends linearly on the Ce content ($\frac{da}{dy} = -4.71(5) \times 10^{-4}$, $R^2 = 0.952$, figure 10, dashed line). The slope is significantly larger than the one observed for the majority phase. Antonio et al. [38] did not observe a signal at the XANES absorption edge of $U_{0.33}Ce_{0.67}O_2$ (Ce: L_3-edge, U: M_5-edge), associated with Ce^{III}, nor any anomalous signal which could be associated with anything but U^{IV}. Thus, we assume that those increased lattice parameters are caused by an incomplete oxidation of Ce^{III} during the calcination, or by a partial reduction of Ce^{IV} to Ce^{III} [29]. The charge imbalance caused by Ce^{III} might be compensated by the formation of oxygen vacancies, leading to a hypo-stoichiometric phase with elevated lattice parameters [39]. This would explain the fact that the microspheres with biphasic compositions did not remain in the spherical shape and broke apart during the sintering under reducing conditions.

We observed $U_{1-y}Nd_yO_{2\pm x}$ single phase solid solutions for the entire dopant range of the Nd-doped compounds, which is also expected for $U_{1-y}Am_yO_{2\pm x}$ compounds with comparable dopant contents [40], while a phase separation was encountered for Ce-doped compositions (Ce^{III} precursor), agreeing with literature [39]. The latter was also found for Pu containing compositions [41] and shows that Ce is a good substitute to simulate the phase separation in the solid oxide phase. Based on the

oxygen potential applied during the sintering in reducing atmosphere, hypo-stoichiometric solid solutions are expected for all doped products. The oxygen deficiency decreases with increasing dopant content, which is also anticipated for $U_{1-y}Pu_yO_{2\pm x}$ solid solutions. However, less oxygen deficiency is expected for Pu-doped UO_2 compared to Ce-doped UO_2 [42], pointing out that the thermal treatment conditions have to be adjusted for Ce to simulate Pu.

5. Conclusion

Nd- and Ce-doped microspheres with a good sphericity and *Ln* contents up to 30 mol% were successfully synthesised via internal gelation, using trivalent *Ln* precursors, while an incomplete gelation was observed for gels prepared with Ce^{IV} precursors and Ce contents of ≥ 10 mol%. The density of the dried gels depends not only on the gelation conditions but also on the dopant and the oxidation state of its precursor. Comparable densities were determined for un-doped material and Nd-doped gels, while the density for Ce-doped gels was found to be higher. The usage of Ce^{IV} as precursor led to gels with higher densities than those prepared with Ce^{III}. The XRD patterns of the dried gels indicate a successful introduction of the dopant into the $3UO_3{\cdot}2NH_3{\cdot}4H_2O$ matrix, independent of the dopant and the oxidation state of its precursor. For the material prepared with the trivalent precursors, the Nd-doped particles underwent a more pronounced shrinkage during the thermal treatment than the Ce-doped particles, while the shrinkage determined for gels prepared with the Ce^{IV} precursors are about a factor of 0.5 smaller than the ones of the microspheres prepared with Ce^{III}. Despite the high shrinkage ratios, a good sphericity was maintained for the Nd-doped particles, while the less significant shrinkage in the Ce-doped particles (Ce^{III} precursor) resulted in a large fraction of broken particles for higher dopant contents. XRD analyses proved the presence of $U_{1-y}Ln_yO_{2\pm x}$ single phase solid solutions for the sintered Nd-doped particles and the sintered Ce-doped particles (Ce^{IV} precursor). For Ce-doped compositions prepared using the trivalent precursor, two solid solutions were observed for Ce contents > 15 mol%, which relates to the physical stability of those sintered particles, i. e. the large fraction of broken particles. The lattice parameters determined for the single phase solid solutions follow Vegard's law and show a decreasing lattice parameter with increasing dopant content. In the case for the Nd-doped material, different charge compensating mechanisms, depending on the dopant content, were assumed. The gelation and thermal treatment conditions investigated in this study are suitable for the preparation of $U_{1-y}Nd_yO_{2\pm x}$ and $U_{1-y}Ce_yO_{2\pm x}$ single phase solid solutions with Nd contents up to 30 mol% and Ce contents up to 15 mol%, using hexahydrates of the trivalent lanthanides as dopant precursors. Due to the lower metal concentration in the sol, compared to existing IG fabrication studies, the usage of a solution containing the gelation agents is possible. This leads to an improved IG fabrication process in terms of automating and remote handling, which delivers benefits for the production of Pu and/or minor actinide containing UO_2 transmutation fuel.

Acknowledgements

The authors thank K. Vanaken and P. Dries for laboratory assistance, Dr. M. Klinkenberg for SEM analyses of particles from the earlier study, Dr. F. Jutier for OM analyses and support on data processing, and P. Verheyen for ICP-MS measurements. Financial support for this research was provided by the European Commission (project: GENIORS - GEN IV Integrated Oxide fuels Recycling Strategies (755171)) and by the Belgian FPS Economy (project: ASOF - Advanced Separation for Optimal management of spent Fuel).

Data Availability Statement

The data required to reproduce the findings of this study are available to download from the repository *zenodo* [22].

References

[1] M. A. Pouchon, G. Ledergerber, F. Ingold, K. Bakker, Sphere-Pac and VIPAC Fuel, in: R. J. Konings (Ed.), Comprehensive Nuclear Materials, Elsevier BV, Oxford, 2012, pp. 275–312. doi:10.1016/b978-0-08-056033-5.00059-8.

[2] S. Suryanarayana, N. Kumar, Y. R. Bamankar, V. N. Vaidya, D. D. Sood, Fabrication of UO_2 pellets by gel pelletization technique without addition of carbon as pore former, Journal of Nuclear Materials 230 (1996) 140–147. doi:10.1016/0022-3115(96)00162-6.

[3] R. D. Shannon, Revised effective ionic radii and systematic studies of interatomic distances in halides and chalcogenides, Acta Crystallographica Section A 32 (1976) 751–767. doi:10.1107/S0567739476001551.

[4] D. Lundberg, I. Persson, The size of actinoid (III) ions–structural analysis vs. common misinterpretations, Coordination Chemistry Reviews 318 (2016) 131–134. doi:10.1016/j.ccr.2016.04.003.

[5] K. Suresh Kumar, H. P. Nawada, N. P. Bhat, Comparative study of thermal decomposition of the sol–gel products of U and Ce by external and internal gelation processes, Journal of Nuclear Materials 321 (2003) 263–268. doi:10.1016/S0022-3115(03)00278-2.

[6] J. L. Collins, A. Chi, Determination of Ideal Broth Formulations Needed to Prepare Hydrous Cerium Oxide Microspheres via the Internal Gelation Process, Technical Report ORNL/TM-2006/122, Oak Ridge National Laboratory (ORNL), 2008. doi:10.2172/947141.

[7] R. D. Hunt, J. L. Collins, J. A. Johnson, B. S. Cowell, Production of 75–150 μm and <75 μm of cerium dioxide microspheres in high yield and throughput using the internal gelation process, Annals of Nuclear Energy 105 (2017) 116–120. doi:10.1016/j.anucene.2017.03.010.

[8] J. A. Katalenich, B. B. Kitchen, B. D. Pierson, Production of monodisperse cerium oxide microspheres with diameters near 100 μm by internal-gelation sol–gel methods, Journal of Sol-Gel Science and Technology 86 (2018) 329–342. doi:10.1007/s10971-018-4641-y.

[9] W. Tian, M. Pouchon, H. Guo, D. Chen, X. Yin, Z. Qin, Fabrication of CeO_2 ceramic spheres as a surrogate of nuclear fuel by an improved microwave-assisted rapid internal gelation process, Ceramics International 44 (2018) 6739–6746.

[10] J. A. Katalenich, Production of cerium dioxide microspheres by an internal gelation sol–gel method, Journal of Sol-Gel Science and Technology (2017) 1–10. doi:10.1007/s10971-017-4345-8.

[11] C. Schreinemachers, G. Leinders, G. Modolo, M. Verwerft, K. Binnemans, T. Cardinaels, The conversion of ammonium uranate prepared via sol-gel synthesis into uranium oxides, Nuclear Engineering and Technology (2019). doi:10.1016/j.net.2019.11.004.

[12] V. N. Vaidya, S. K. Mukherjee, J. K. Joshi, R. V. Kamat, D. D. Sood, A study of chemical parameters of the internal gelation based sol-gel process for uranium dioxide, Journal of Nuclear Materials 148 (1987) 324–331. doi:10.1016/0022-3115(87)90026-2.

[13] A. Kumar, J. Radhakrishna, N. Kumar, R. V. Pai, J. V. Dehadrai, A. C. Deb, S. K. Mukerjee, Studies on preparation of $(U_{0.47},Pu_{0.53})O_2$ microspheres by internal gelation process, Journal of Nuclear Materials 434 (2013) 162–169. doi:10.1016/j.jnucmat.2012.11.009.

[14] C. Schreinemachers, A. A. Bukaemskiy, M. Klinkenberg, S. Neumeier, G. Modolo, D. Bosbach, Characterization of uranium neodymium oxide microspheres synthesized by internal gelation, Progress in Nuclear Energy 72 (2014) 17–21. doi:10.1016/j.pnucene.2013.07.016.

[15] P. A. Haas, J. M. Begovich, A. D. Ryon, J. S. Vavruska, Chemical flowsheet conditions for preparing urania spheres by internal gelation, Technical Report ORNL/TM-6850, Oak Ridge National Laboratory (ORNL), 1979. doi:10.2172/6104596.

[16] T. B. Lindemer, T. M. Besmann, Chemical thermodynamic representation of $UO_{2\pm x}$, Journal of Nuclear Materials 130 (1985) 473–488. doi:10.1016/0022-3115(85)90334-4.

[17] G. Leinders, T. Cardinaels, K. Binnemans, M. Verwerft, Accurate lattice parameter measurements of stoichiometric uranium dioxide, Journal of Nuclear Materials 459 (2015) 135–142. doi:10.1016/j.jnucmat.2015.01.029.

[18] J. Schindelin, I. Arganda-Carreras, E. Frise, V. Kaynig, M. Longair, T. Pietzsch, S. Preibisch, C. Rueden, S. Saalfeld, B. Schmid, J.-Y. Tinevez, D. J. White, V. Hartenstein, K. Eliceiri, P. Tomancak, A. Cardona, Fiji: an open-source platform for biological-image analysis, Nature Methods 9 (2012) 676–682. doi:10.1038/nmeth.2019.

[19] J. B. Nelson, D. P. Riley, An experimental investigation of extrapolation methods in the derivation of accurate unit-cell dimensions of crystals, Proceedings of the Physical Society 57 (1945) 160–177. doi:10.1088/0959-5309/57/3/302.

[20] H. M. Rietveld, A profile refinement method for nuclear and magnetic structures, Journal of Applied Crystallography 2 (1969) 65–71. doi:10.1107/S0021889869006558.

[21] M. Wojdyr, Fityk: a general-purpose peak fitting program, Journal of Applied Crystallography 43 (2010) 1126–1128. doi:10.1107/s0021889810030499.

[22] C. Schreinemachers, G. Leinders, Characterisation data of Nd- and Ce-doped uranium dioxide microspheres prepared via internal gelation, 2020. doi:10.5281/zenodo.3560620, (Version 1.0.0) [Data set], License: CC BY-NC.

[23] C. Schreinemachers, Preparation and characterization of U/Nd microspheres synthesized by internal gelation, Msc thesis, Fachhochschule Aachen, Campus Jülich, 2013. doi:10.5281/zenodo.3250624.

[24] C. Schreinemachers, G. Leinders, Thermal decomposition data of uranium containing microspheres produced via internal gelation and ammonium diuranate powder, 2019. doi:10.5281/zenodo.3250894, (Version 1.0.0) [Data set], License: CC BY-NC-SA.

[25] J. Härtwig, G. Hölzer, E. Förster, K. Goetz, K. Wokulska, J. Wolf, Remeasurement of characteristic X-ray emission lines and their application to line profile analysis and lattice parameter determination, physica status solidi (a) 143 (1994) 23–34. doi:10.1002/pssa.2211430104.

[26] J. K. Fink, Thermophysical properties of uranium dioxide, Journal of Nuclear Materials 279 (2000) 1–18. doi:10.1016/S0022-3115(99)00273-1.

[27] R. D. Hunt, J. L. Collins, M. H. Lloyd, S. C. Finkeldei, Production of more ideal uranium trioxide microspheres for the sol-gel microsphere pelletization process without the use of carbon, Journal of Nuclear Materials 515 (2019) 107–110. doi:10.1016/j.jnucmat.2018.12.029.

[28] J. L. Collins, M. F. Lloyd, R. L. Fellows, The basic chemistry involved in the internal-gelation method of precipitating uranium as determined by pH measurements, Radiochimica Acta 42 (1987) 121–134. doi:10.1524/ract.1987.42.3.121.

[29] Y.-K. Ha, J. Lee, J.-G. Kim, J.-Y. Kim, Effect of Ce doping on UO_2 structure and its oxidation behavior, Journal of Nuclear Materials 480 (2016) 429–435. doi:10.1016/j.jnucmat.2016.08.026.

[30] R. Bès, K. Kvashnina, A. Rossberg, G. Dottavio, L. Desgranges, Y. Pontillon, P. Solari, S. Butorin, P. Martin, New insight in the uranium valence state determination in $U_yNd_{1-y}O_{2\pm x}$, Journal of Nuclear Materials 507 (2018) 145–150. doi:10.1016/j.jnucmat.2018.04.046.

[31] K. Une, M. Oguma, Oxygen potentials of (U,Nd)$O_{2\pm x}$ solid solutions in the temperature range 1000 – 1500 °C, Journal of Nuclear Materials 118 (1983) 189–194. doi:10.1016/0022-3115(83)90224-6.

[32] J. F. Wadier, Diagramme de phases et proprietes thermodynamiques du systeme uranium-neodyme-oxygene, Technical Report CEA-R-4507, Commissariat à l'énergie atomique, 1973.

[33] T. Ohmichi, S. Fukushima, A. Maeda, H. Watanabe, On the relation between lattice parameter and O/M ratio for uranium dioxide-trivalent rare earth oxide solid solution, Journal of Nuclear Materials 102 (1981) 40–46. doi:10.1016/0022-3115(81)90544-4.

[34] S. M. Lee, T. W. Knight, S. L. Voit, R. I. Barabash, Lattice parameter behavior with different Nd and O concentrations in $(U_{1-y}Nd_y)O_{2\pm x}$ solid solution, Nuclear Technology 193 (2016) 287–296. doi:10.13182/NT14-136.

[35] B. E. Hanken, T. Y. Shvareva, N. Gronbech-Jensen, C. R. Stanek, M. Asta, A. Navrotsky, Energetics of cation mixing in urania-ceria solid solutions with stoichiometric oxygen concentrations, Phys. Chem. Chem. Phys. 14 (2012) 5680–5685. doi:10.1039/C2CP40295E.

[36] R. Venkata Krishnan, G. Panneerselvam, B. M. Singh, B. Kothandaraman, G. Jogeswararao, M. Antony, K. Nagarajan, Synthesis, characterization and thermal expansion measurements on uranium–cerium mixed oxides, Journal of Nuclear Materials 414 (2011) 393–398. doi:10.1016/j.jnucmat.2011.05.010.

[37] S. Sali, M. Keskar, R. Phatak, K. Krishnan, G. P. Shelke, P. M. Shafeeq, S. Kannan, Oxidation behavior of $(U_{1-y}Ce_y)O_{2.00}$; (y = 0.21, 0.28 and 0.44) solid solutions under different oxygen potentials. Thermogravimetric and in situ X-ray diffraction studies, Journal of Nuclear Materials 510 (2018) 499–512. doi:10.1016/j.jnucmat.2018.08.043.

[38] M. R. Antonio, U. Staub, J. S. Xue, L. Soderholm, Comparison of the cation valence and coordination in Ce_2UO_6 and Ce_2MoO_6, Chemistry of Materials 8 (1996) 2673–2680. doi:10.1021/cm960208c.

[39] T. Markin, R. Street, E. Crouch, The uranium-cerium-oxygen ternary phase diagram, Journal of Inorganic and Nuclear Chemistry 32 (1970) 59–75. doi:10.1016/0022-1902(70)80449-3.

[40] T. Nishi, M. Nakada, M. Hirata, Lattice parameter functions of $(Am_yU_{1-y})O_{2-x}$ based on XRD and XANES measurements, Journal of Solid State Chemistry 256 (2017) 252–255. doi:10.1016/j.jssc.2017.09.011.

[41] R. Vauchy, R. C. Belin, A.-C. Robisson, F. Hodaj, High temperature X-ray diffraction study of the kinetics of phase separation in hypostoichiometric uranium–plutonium mixed oxides, Journal of the European Ceramic Society 34 (2014) 2543–2551. doi:10.1016/j.jeurceramsoc.2014.02.028.

[42] T. B. Lindemer, J. Brynestad, Review and chemical thermodynamic representation of $U_{1-z}Ce_zO_{2\pm x}$ and $U_{1-z}Ln_zO_{2\pm x}$; *Ln* = Y, La; Nd, Gd, Journal of the American Ceramic Society 69 (1986) 867–876. doi:10.1111/j.1151-2916.1986.tb07386.x.